# High-Performance $Bi_2Te_3$-Based Topological Insulator Film Magnetic Field Detector

H. B. Zhang,[†,‡] H. Li,[†] J. M. Shao,[†] S. W. Li,[†] D. H. Bao,[†] and G. W. Yang*,[†]

[†]State Key Laboratory of Optoelectronic Materials and Technologies, Institute of Optoelectronic and Functional Composite Materials, Nanotechnology Research Center, School of Physics & Engineering, Sun Yat-sen University, Guangzhou, Guangdong 510275, P. R. China

[‡]Institute of Functional Nano & Soft Materials (FUNSOM), Jiangsu Key Laboratory for Carbon-Based Functional Materials & Devices, Soochow University, Suzhou, Jiangsu 215123, P. R. China

**ABSTRACT:** Topological insulators with the nanoscaled metallic surface state (3–5 nm) are actually of typical functional nanostructures. Significant efforts have been devoted to study new families of topological insulators and identifications of topological surface state, as well as fundamental physics issues relating to spin-polarized surface electronic states in the past few years. However, transport investigations that can provide direct experimental evidence for potentially practical applications of topological insulators are limited, and realization of functional devices based on topological insulators is still under exploration. Here, using the Sn-doping $Bi_2Te_3$ polycrystalline topological insulator films, we fabricated high-performance current-controlled magnetic field detectors. When a parallel magnetic field is applied, the as-fabricated device exhibits a stable and reproducible magneto-resistance (MR) switching behavior, and the corresponding MR ratio can be modulated by the applied current. Even under such a low magnetic field (0.5 kG), the device still shows a distinguishable MR switching performance, suggesting that topological insulator devices are very sensitive to external stimulation and potentially applicable to weak magnetic field detection.

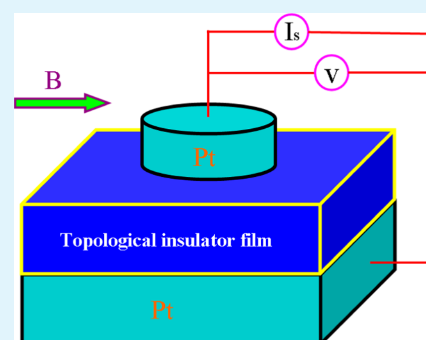


**KEYWORDS:** *topological insulator, magnetic-field detector*

The topological insulator characterized by an insulating bulk and a conductive surface (3–5 nm) with a Dirac-like linear dispersion has demonstrated a wide range of fascinating quantum phenomena and potentially technical applications.[1−8] Therefore, the topological insulator is actually of typical functional nanostructures. In the past few years, significant efforts have been devoted to search new families of topological insulators and the identifications of the topological surface state, as well as the fundamental physics issues relating to the spin-polarized surface state.[9−17] Among topological insulator materials, the $Bi_2Te_3$ compound was first proposed to be one of the three-dimensional topological insulator materials with a perfectly linear Dirac cone on its surface by theoretical band structure calculations,[4] and such topologically nontrivial surface state was then verified experimentally by the surface-sensitive techniques of angle-resolved photoemission spectroscopy and scanning tunneling spectroscopy.[9−11] In transport experiments, the important weak antilocalization feature and the quantum oscillation effects such as the surface Shubnikov–de Haas oscillations and Aharonov–Bohm oscillations observed in their magnetoresistance (MR) curves have been identified arising from the surface Dirac fermions.[12−16] Recently, the experimental observations of the quantum anomalous Hall effect were reported in magnetically doped topological insulator ultrathin films.[18] However, the transport investigations that can provide direct experimental evidence for the potential practical applications of topological insulators are limited and the realizations of functional devices of topological insulators are still under exploration. For this issue, in this contribution, we fabricate the high-performance current-controlled magnetic field detectors made from the Sn-doped $Bi_2Te_3$ topological insulator polycrystalline films on the basis of the systematic magneto-transport investigations.[7,19] The magnetic-field detector in this study is a unit cell fabricated on the basis o fthe Pt/topological insulator/Pt structure with the size of micrometer order. The characterizations of the as-fabricated device have showed that the topological insulator detectors are very sensitive to the external stimulation and potentially applicable to magnetic sensors and logics, magnetic random access memories, read heads in hard disk drives, and so on.

Because of the huge tunneling MR ratio (100% or more) in the magnetic tunnel junctions, they can generally be used as the magnetic field detection device. However, a magnetic tunnel junction typically consists of a FM1/I/FM2 structure, where FM1 and FM2 are two ferromagnetic contacts and I is a thin layer of insulating material. Its MR ratio depends on the electronic properties of both electrodes, so it requires the very harsh junction quality including the optimized material,

Received: August 27, 2013
Accepted: October 30, 2013
Published: October 30, 2013

 © 2013 American Chemical Society 

structure, and growth conditions. On the other hand, the insulating materials in the magnetic tunnel junctions have large band gaps, and the junction resistance is typically very large. As a result, for a given current the power dissipation is high, which seriously degrades the reliability of the magnetic-field detector and limits its application in the low-power consumption region.[20,21] The maganites are known to exhibit the colossal MR effect, which enables the materials to dramatically change their electrical resistance in the presence of a magnetic field. As an external field of some Tesla is applied, the magnetic order is enhanced and the resistivity can be decreased by several orders of magnitude. However, the colossal MR effect generally has a strongly temperature dependence, and the largest MR for the manganites usually appears near the Curie temperature $T_C$.[22,23] Compared to the conventional high-mobility semiconductor materials which MR usually exhibits a quadratic dependence on the magnetic field at low fields but saturating at high fields, an anomalously large and nonsaturating linear MR behavior was observed in InSb and $Ag_2Te$ materials, and the MR ratio is comparable with the colossal-MR materials. More importantly, the MR is weakly temperature dependent and linear down to very low fields. Although the linear MR response is more suitable for practical application in the field of magnetic field detection, it is still based on the large positive MR effect.[24−26]

Although most commonly used magnetic-field detectors by far are Si-based Hall devices, which exploit the galvanomagnetic effects to transform a magnetic signal into an electric signal because of the Lorentz force on the charge carriers, these devices are difficult to manufacture and hard to be integrated with signal-processing circuits.[27,28] Considering the topological insulator is a novel quantum material which possesses many intrinsic quantum magneto-transport properties, we try to explore the possible device applications of topological insulator films in the field of magnetic-field detection. The surprise in our case is that the experimentally observed MR of the samples shows the pronounced quasi-linear and negative MR response which reflecting new physical mechanism, and such state is of great importance in low power magnetic detector. In addition, because of the small size, low power consumption, and sensitivity, the new detector could be easily grouped in arrays, and make it possible to gain more data in a given amount of time.

Generally, topological insulators are the materials characterized by an insulating bulk and a conductive surface. The hallmark of a topological insulator is its linearly dispersing surface state which is guaranteed by the time-reversal symmetry, and thus cannot be destroyed by any nonmagnetic impurities. The surface state has a chiral spin texture, which offers the electrons protection against backscattering, and the strong spin−orbit coupling in the surface state of topological insulators results in the ubiquitously observed weak antilocalization feature in MR.[19] Besides, the bulk channels of the topological insulators can also become quantized due to the different scattering mechanism in the bulk state, and an additional negative MR feature may appear associated with the weak localization effect of the quantized bulk channels.[19] Therefore, to exploit these phenomena, we present MR measurements in the topological insulator films of Sn-doped $Bi_2Te_3$ and show the high-performance current-controlled magnetic-field detectors based on the special MR behavior.

In this study, the Sn-doped $Bi_2Te_3$ polycrystalline topological insulator films are prepared in a high-vacuum growth chamber via the pulsed laser deposition, and all the topological insulator films are deposited on the $Pt/TiO_2/SiO_2/Si$ wafers with an optimized substrate temperature of 300 °C. The base pressure of the deposition chamber is better than $1.0 \times 10^{-4}$ Pa and the working pressure is set at 40 Pa, with 50 sccm of Ar flowing as the working gas. The target material consisting of high-purity Bi (99.999%) and Te (99.999%) with a Bi/Te molar ratio of 2:3 is used as the source to grow the $Bi_2Te_3$ topological insulator films. In order to suppress the bulk-state conductivity in the undoped films, we chose to prepare the $Bi_2Te_3$ films with the high-purity Sn (99.999%) doping, and the Sn doping concentration can be systematically tuned through controlling the Sn content in target materials.

For fabricating a magnetic field detector, the Pt top electrode with a diameter of 300 $\mu$m is then deposited on the surface of the $Bi_2Te_3$ film as the Ohmic contact electrode. The top electrode is prepared at room temperature by sputtering technique patterned with a shadow mask. The transport measurements are carried out by a Keithley 4200-SCS semiconductor characterization system combined with a probe station under a dc measurement technique with a two-probe configuration at room temperature. The current−voltage characteristics of the fabricated devices show the linear Ohmic behavior, which indicating a good electrical contact to the topological insulator films. In the magneto-transport measurements, a constant current is injected into the top Pt electrode, and the voltage signal across the top and bottom electrodes is collected to determine its resistance. Meanwhile, the magnetic field is applied parallel to the device plane but perpendicular to the direction of the injected current, and the applied parallel field is a conventional magnetic field located on our probe station, which is excited by a direct-current coil.

Figure 1a shows the schematic diagram of the fabricated detector. Note that our measurements show that only the $Bi_2Te_3$ film with an appropriate Sn doping can present the remarkable MR switch effect under an applied parallel field. As plotted in Figure 1b, the detector is initially in a high-resistance state, but the resistance shows a downward jump and then turns into the low-resistance state when a parallel field is applied. However, as the applied parallel field vanishes, the device starts going back into its high-resistance state until the parallel magnetic field is applied again. Thus, the transport data show that the MR switching behavior is actually a negative quantum MR effect.

Compared to the undoped topological insulator samples, doping Sn atoms into $Bi_2Te_3$ can effectively reduce the bulk-state resistance of the topological insulator films. In fact, the as-grown undoped stoichiometric $Bi_2Te_3$ films usually possess a finite density of Te vacancies and antisite defects, which act as an electron donor and make the Fermi level pin within the bulk conduction band (producing a large number of the bulk-state carriers). Additionally, the Sn dopant as an acceptor has already been proven to be effective in tuning the bulk carrier type, and can lead to a downshift of the Fermi level.[9,27] By doping the $Bi_2Te_3$ films within an intermediate Sn concentration, the Fermi level of our samples can be lowered into the bulk band gap from the bulk conduction band, which results in a relatively insulating bulk-state resistance.[19] Meanwhile, through systematic experimental investigation, we find that the prepared film which presents the pronounced MR switch feature is usually accompanied with a relatively large bulk resistance. Thus, in this study, we mainly focus on the magnetic detector fabricated by the Sn-doped $Bi_2Te_3$ topological insulator film with the minimal bulk conduction, and the corresponding thickness of

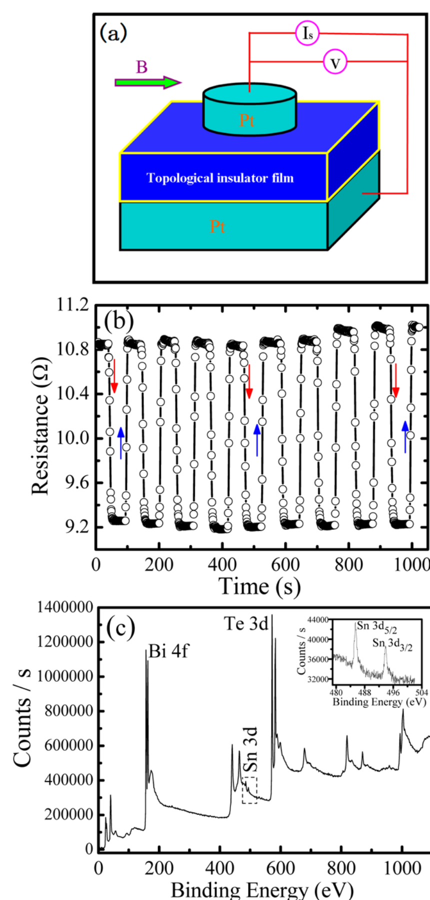


**Figure 1.** (a) Schematic diagram of the detector fabricated with the Sn-doped $Bi_2Te_3$ topological insulator film and the corresponding measurement circuit. (b) MR switching performance taken at $I_s$ = 10 mA and $B$ = 3.0 kG. (c) Typical XPS profile of Sn-doped $Bi_2Te_3$ films. The inset shows the presence of Sn in $Bi_2Te_3$.

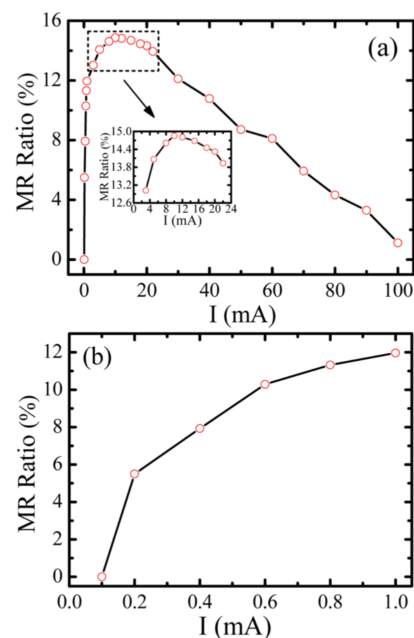


**Figure 2.** (a) Current-induced change of the MR ratio acquired under a parallel magnetic field of 3.0 kG and room temperature. (b) Zoomed-in view of the MR ratio evolution taken in the low-current injection region.

the film is about 300 nm. The actual chemical composition of the Sn-doped $Bi_2Te_3$ film is also studied by the X-ray photoelectron spectroscopy (XPS), and the corresponding spectra are shown in Figure 1c. The typical XPS profile in the inset of Figure 1c shows the presence of the Sn element, and the doping concentration of Sn in the $Bi_2Te_3$ topological insulator films which exhibits the most significant MR switch property is determined to be ∼1.5%. Thus under the optimized Sn doping condition, the Fermi level of the Sn-doped $Bi_2Te_3$ film should be located in the bulk band gap. However, the measured bulk resistance of the Sn-doped $Bi_2Te_3$ film appears to be not sufficiently large, and the carrier density of the film is in the range of $1 \times 10^{18}$ cm$^{-3}$. Thus, the expected truly bulk-insulating state seems not to be achieved so far. The residual bulk conductance of the film is probably due to the formation of a Sn-related impurity band, which is attributed to the acceptor levels and may located inside the bulk band gap.[29,30] Therefore, the qualitative analysis reveals that the Fermi level of the Sn-doped $Bi_2Te_3$ film is not only lowered into the bulk energy gap, but also pinned to the impurity band.

We then study the influence of the injected current on the MR switch property of the detector as shown in Figure 2. Although we observe a negative MR effect during our transport experiments, according to the traditional custom, we define the MR variation as a positive percentage. Thus the practical MR ratio is defined as $\Delta MR\% = 100 \times [R(0) - R(H)]/R(0)$, where $R(H)$ and $R(0)$ are the resistance taken with and without the magnetic field, respectively. The relative error of the MR ratio in this study is less than 5%. Clearly, the MR ratio possesses a nonmonotonic variation with the injected current, and reaches a peak of 14.86% at 10 mA, and then decreases with the injected current increasing. In Figure 2a, the MR ratio acquired from the low-current region rises rapidly with the injected current increasing. On the contrary, the MR ratio starts to be gradually suppressed in the high-current region that the injected current is greater than 10 mA. Thus, these results confirm that the MR switching performance of the detector can be easily controlled by the injected current. Meanwhile, for each applied parallel field, there exists an optimal value of the injected current, which makes the detector work in the most notable MR switching performance.

To further examine the practical performance of the detector under the fixed excitation currents, we study the actual MR response of the device varying with the applied parallel field under the selected injection current 100, 40, 10, 1.0, and 0.3 mA, respectively. The corresponding evolution of the MR ratio as a function of the magnetic-field strength is plotted in Figure 3a. Clearly, the MR ratio exhibits the qualitatively consistent trends and rises monotonically with the magnetic field increasing. Besides, under the optimized current of 10 mA, the MR ratio shows the significant transient response to the external magnetic field and reaches a maximal value of 36.25% at 5.5 kG (the highest magnetic-field that can be achieved in our probe station).

Additionally, the MR switching response of the detector under the optimized current of 10 mA and a weak magnetic field of 0.5 kG is investigated in detail, as shown in Figure 3b. The results indicate that even in such a low external field, the device still presents a distinguishable MR switch performance, which suggests that the fabricated detector not only has high detection sensitivity, but also is very sensitive to the external magnetic field stimulation. Note that the longer exposure time

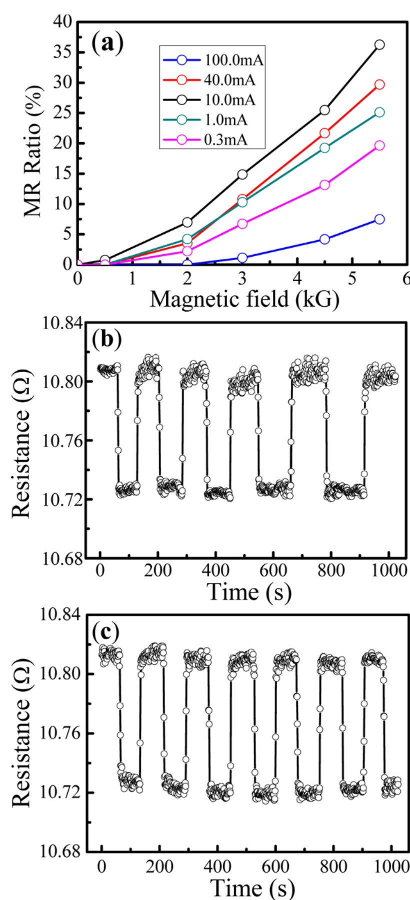


**Figure 3.** (a) MR ratio measured under the selected excitation currents plotted as a function of the parallel magnetic field *B*. (b) Distinguishable MR switching characteristic of the device detected under the injected current of 10 mA and a weak magnetic field of 0.5 kG. (c) MR switching response of the detector measured under exactly the same conditions as described in b but several weeks later.

of the topological insulator films in air may result in the degradation of the topological surface state by possible organic or water molecule contamination, and the degradation of the device performance may occur. However, in our device, it hardly affects the reliability of the MR switching feature based on our designed device structure, because the Pt electrode covered on the film surface can be used as the protective layer, which prevents the topological insulator film from direct exposure to the atmosphere. The corresponding MR data measured under the same conditions as described for Figure 3b but after several weeks is demonstrated in Figure 3c. Thus, these experimental results reveal that the novel MR switching behavior of the detector can be stably maintained under the atmospheric condition.

Because of the good application prospect in the field of magnetic-field detection, it is necessary to do an in-depth study on the injected current modulation of the MR switching behavior under a variety of external magnetic fields. In order to facilitate the observation and analysis, the current-controlled MR responses under the selected parallel fields are expressed in two different injection current regions, i.e., the MR ratio evolution of the device measured at the low current injection level as shown in Figure 4a, and the current dependence of the MR ratio taken within the high injected current range in Figure 4b. Clearly, the evolution trends of the MR ratio along with the injection current under the fixed magnetic fields take on the qualitatively consistent feature in each of the two current regions, which also reveals the similar modulating effect of the injected current on the MR behavior in their respective regions.

Compared to the current modulating response in the weak magnetic fields, the modulating performance of the injected current in the strong fields becomes even more significant and sensitive. Under the high magnetic-field conditions, with the injected current varying, the corresponding variation of the MR ratio is greatly increased. In addition, as the magnetic-field increases, the adjustable range of the injected current gets larger correspondingly as shown in Figure 4b. Well known, the large value of the MR ratio is a basic parameter of a magnetic field detector, which is directly related to the detection sensitivity and affects the practical performance of the device.[28] Because the MR ratio of our fabricated detector can be strictly controlled by the injected current under each field condition during the transport measurements, the detection sensitivity of the device should be effectively regulated by the exciting current, and the corresponding MR switching performance can be greatly improved.

The significant modulating effect of the injected current on the MR ratio is attributed to the intrinsic transport property of the Sn-doped $Bi_2Te_3$ topological insulator film. In our transport experiments, when an external excitation current is injected from the Pt top electrode as shown in Figure 1a, the positive electric potential is set up properly, and the build-up potential distributes perpendicularly to the device plane, which can not only shift the surface Dirac linear dispersion vertically, but also produce the strongly downward band bending of the bulk bands toward the film surface.[31,32] The schematic diagrams of the surface Dirac linear dispersion and the bulk bands along the depth of the film are shown in Figure 4c, and Figure 4d describes the typical downward band bending of the insulating bulk state relative to the topological surface state near the film surface affected by the built-up potential. Thus, this downward band bending effect tends to develop the bulk-state electrons on the $Bi_2Te_3$ topological insulator surface layer, which can make the topological surface state electrons and bulk state carriers coherent coupling during the transport process.[31−33] Once the gapless singlet cooperon from the bulk state couples strongly with the gapless singlet cooperon on the topological surface state, the bulk-state and surface-state electrons will behave together as a single phase coherent weak antilocalization (WAL) transport channel due to the destructive quantum interference in the time-reversed scattering paths induced by the strong spin-momentum coupling effect, which makes each coupling transport channel contribute the positive quantum correction to the classical resistance.[31−34] Thus, under the lowest current injection level as shown in Figure 4a, the practical MR switch feature of the detector seems missing, i.e., the observed negative MR behavior turns to be suppressed. Therefore, at lower current conditions, the coherent coupling WAL transport channels are prevalent and the contribution of the WAL quantum correction becomes significant in the overall transport properties.[19,35]

However, with the injected current rising, more and more bulk-state carriers will involve in the completely decoupling transport regime. In other words, the carriers in the surface and bulk channels lose the phase coherence before being scattered into the other. Thus, under our well-defined measurement configuration, the surface-state and bulk-state electrons are contributing in series, and because of the relatively large bulk

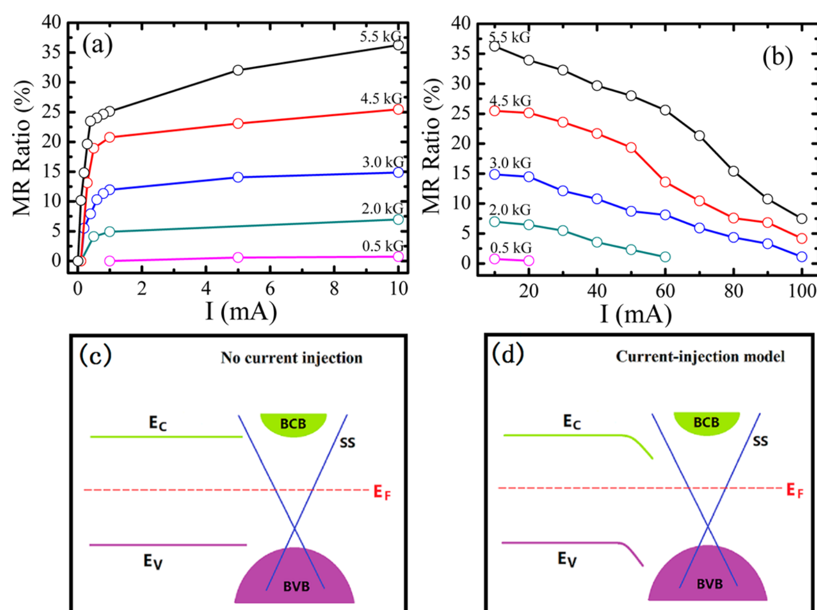


**Figure 4.** Modulating effect of the injected current on the MR ratio under different magnetic field conditions: (a) low-current injection region of $I_s \leq$ 10 mA and (b) high-current injection region of $I_s \geq$ 10 mA. Schematic band structure of a topological insulator film: (c) No current-injection condition and (d) current injection model. The right-hand side shows the linear energy-momentum dispersion of the surface state (SS), which exists in the gap between the bulk conduction band (BCB) and the bulk valence band (BVB). The left-hand side indicates the typical downward band bending of the bulk conduction band minimum ($E_C$) and the bulk valence band maximum ($E_V$) relative to the Fermi level ($E_F$) toward the film surface.

resistance, the bulk transport channels actually dominate the total transport property of the film.[31] In contrast to the gapless surface state, the bulk state of the $Bi_2Te_3$ topological insulator has a relatively large bulk band gap. Thus, under the strong elastic scattering induced by the Sn impurities, the decoupling bulk channels can be driven into the weak localization (WL) quantum diffusion transport mechanismbecause of the constructive quantum interference of the time-reversed self-intersecting scattering paths.[19,35] Thus, it provides a negative quantum correction to the classical resistance, and is directly consistent with the observed novel MR switching feature in our detector. As the injecting current continuously increases, the proportion of the decoupling WL transport channels increases rapidly, and the WL quantum correction effect gradually becomes predominant, which leading to more and more pronounced MR switching feature in our detector.

When the injected current increases to the optimized value of 10 mA, the bulk state of the film is almost completely decoupled from the topological surface state, and the overall magneto-transport of the device may locate in the fully WL quantum diffusion transport regime, which also corresponds to the most significant MR switching feature of the designed detector. However, under the parallel field configuration in this study, the isolated topological surface state gives virtually no contribution to the MR switching behavior. The main reason is that the topological surface state only responds strongly to a perpendicular magnetic field. Under the perpendicular field conditions, the surface Dirac linear dispersion can be quantized into the Landau levels and open up a band gap at the Dirac point, which can result in a positive quantum correction to the classical transport.[19,36,37] Note that the isolated topological surface state does not respond to a static parallel field except a rigid shift in momentum space, because the corresponding term in the Hamiltonian can be eliminated.[38,39]

In the high-current injection region as shown in Figure 4b, the opposite trend of the MR ratio is observed for the detector, and the corresponding MR ratio starts to decline with increasing the injected current. Because under the higher current conditions, a large number of decoupled bulk-state electrons will contribute simultaneously to the transport process, the direct interband coupling or scattering among the bulk sub-bands can reduce the phase coherence length, which leading to the suppression of the WL quantum correction to transport.[35,40−42] Besides, the inelastic electron−phonon scattering in the bulk channels can be greatly enhanced as well with the current increasing, which also lead to the phase decoherence for the time-reversed self-intersecting loops. Thus, as demonstrated in Figure 4b, the actual MR ratio of the detector monotonically decreases with the rise of the injected current in each field condition. As a result, the desired MR switching property of the device may not be able to survive when the injection current becomes too large, and the total magneto-transport of the topological insulator films will be finally driven into the classical diffusion transport regime.

In summary, we have demonstrated high-performance current-controlled magnetic field detectors made from the Sn-doped $Bi_2Te_3$ polycrystalline topological insulator films. In these novel magnetic field detectors, the practical MR switching performance is strictly controlled by the injected current, and there exists an optimal injection current for each applied magnetic field. The significant modulating effect of the injected current on the MR ratio is attributed to a series of the transport evolution from the surface-to-bulk coupling transport regime to the decoupling WL-dominated bulk transport mechanism and finally into the classical diffusion transport. These unique properties of topological insulators enable the fabricated devices are very sensitive to the external stimulation and applied to the weak magnetic field (0.5 kG) detection.

## AUTHOR INFORMATION

### Corresponding Author

*E-mail: stsygw@mail.sysu.edu.cn.

### Notes

The authors declare no competing financial interest.

## ACKNOWLEDGMENTS

This work was supported by the State Key Laboratory of Optoelectronic Materials and Technologies of Sun Yat-sen University.

## REFERENCES

(1) Qi, X.-L.; Zhang, S.-C. *Rev. Mod. Phys.* **2011**, *83*, 1057−1110.
(2) Hasan, M. Z.; Kane, C. L. *Rev. Mod. Phys.* **2010**, *82*, 3045−3067.
(3) Roushan, P.; Seo, J.; Parker, C. V.; Hor, Y. S.; Hsieh, D.; Qian, D.; Richardella, A.; Hasan, M. Z.; Cava, R. J.; Yazdani, A. *Nature* **2009**, *460*, 1106−1109.
(4) Zhang, H.; Liu, C.-X.; Qi, X.-L.; Dai, X.; Fang, Z.; Zhang, S.-C. *Nat. Phys.* **2009**, *5*, 438−442.
(5) Peng, H.; Dang, W.; Cao, J.; Chen, Y.; Wu, D.; Zheng, W.; Li, H.; Shen, Z.-X.; Liu, Z. *Nat. Chem.* **2012**, *4*, 281−286.
(6) Cho, S.; Butch, N. P.; Paglione, J.; Fuhrer, M. S. *Nano Lett.* **2011**, *11*, 1925−1927.
(7) Zhang, H. B.; Yu, H. L.; Bao, D. H.; Li, S. W.; Wang, C. X.; Yang, G. W. *Adv. Mater.* **2012**, *24*, 132−136.
(8) Wang, X.; Du, Y.; Dou, S.; Zhang, C. *Phys. Rev. Lett.* **2012**, *108*, 266806.
(9) Chen, Y. L.; Analytis, J. G.; Chu, J.-H.; Liu, Z. K.; Mo, S.-K.; Qi, X. L.; Zhang, H. J.; Lu, D. H.; Dai, X.; Fang, Z.; Zhang, S. C.; Fisher, I. R.; Hussain, Z.; Shen, Z.-X. *Science* **2009**, *325*, 178−181.
(10) Zhang, T.; Cheng, P.; Chen, X.; Jia, J.-F.; Ma, X.; He, K.; Wang, L.; Zhang, H.; Dai, X.; Fang, Z.; Xie, X.; Xue, Q.-K. *Phys. Rev. Lett.* **2009**, *103*, 266803.
(11) Alpichshev, Z.; Analytis, J. G.; Chu, J.-H.; Fisher, I. R.; Chen, Y. L.; Shen, Z. X.; Fang, A.; Kapitulnik, A. *Phys. Rev. Lett.* **2010**, *104*, 016401.
(12) Qu, D.-X.; Hor, Y. S.; Xiong, J.; Cava, R. J.; Ong, N. P. *Science* **2010**, *329*, 821−824.
(13) Peng, H.; Lai, K.; Kong, D.; Meister, S.; Chen, Y.; Qi, X.-L.; Zhang, S.-C.; Shen, Z.-X.; Cui, Y. *Nat. Mater.* **2010**, *9*, 225−229.
(14) Xiu, F.; He, L.; Wang, Y.; Cheng, L.; Chang, L.-T.; Lang, M.; Huang, G.; Kou, X.; Zhou, Y.; Jiang, X.; Chen, Z.; Zou, J.; Shailos, A.; Wang, K. L. *Nat. Nanotechnol.* **2011**, *6*, 216−221.
(15) Analytis, J. G.; McDonald, R. D.; Riggs, S. C.; Chu, J.-H; Boebinger, G. S.; Fisher, I. R. *Nat. Phys.* **2010**, *6*, 960−964.
(16) He, H.-T.; Wang, G.; Zhang, T.; Sou, I.-K.; Wong, G. K. L.; Wang, J.-N.; Lu, H.-Z.; Shen, S.-Q.; Zhang, F.-C. *Phys. Rev. Lett.* **2011**, *106*, 166805.
(17) Zhang, H. B.; Yu, H. L.; Yang, G. W. *Europhys. Lett.* **2011**, *95*, 56002.
(18) Chang, C.-Z.; Zhang, J.; Feng, X.; Shen, J.; Zhang, Z.; Guo, M.; Li, K.; Ou, Y.; Wei, P.; Wang, L.-L.; Ji, Z.-Q.; Feng, Y.; Ji, S.; Chen, X.; Jia, J.; Dai, X.; Fang, Z.; Zhang, S.-C.; He, K.; Wang, Y.; Lu, L.; Ma, X.-C.; Xue, Q.-K. *Science* **2013**, *340* (6129), 167−170.
(19) Zhang, H. B.; Yu, H. L.; Bao, D. H.; Li, S. W.; Wang, C. X.; Yang, G. W. *Phys. Rev. B* **2012**, *86*, 075102.
(20) Liu, D.; Han, X.; Guo, H. *Phys. Rev. B* **2012**, *85*, 245436.
(21) Liu, R. S.; Yang, S.-H.; Jiang, X.; Zhang, X.-G.; Rettner, C.; Gao, L.; Topuria, T.; Rice, P. M.; Zhang, W.; Canali, C. M.; Parkin, S. S. P. *Phys. Rev. B* **2013**, *87*, 024411.
(22) Coey, J. M. D.; Viret, M.; Molnaír, S. V. *Adv. Phys.* **1999**, *48* (2), 167−293.
(23) Mukherjee, A.; Cole, W. S.; Woodward, P.; Randeria, M.; Trivedi, N. *Phys. Rev. Lett.* **2013**, *110*, 157201.
(24) Xu, R.; Husmann, A.; Rosenbaum, T. F.; Saboungi, M.-L.; Enderby, J. E.; Littlewood, P. B. *Nature* **1997**, *390*, 57−60.
(25) Zhang, W.; Yu, R.; Feng, W.; Yao, Y.; Weng, H.; Dai, X.; Fang, Z. *Phys. Rev. Lett.* **2011**, *106*, 156808.
(26) Hu, J.; Rosenbaum, T. F. *Nat. Mater.* **2008**, *7*, 697−700.
(27) Xu, H.; Zhang, Z.; Shi, R.; Liu, H.; Wang, Z.; Wang, S.; Peng, L.-M. *Sci. Rep.* **2013**, *3*, 1207.
(28) Wan, C.; Zhang, X.; Gao, X.; Wang, J.; Tan, X. *Nature* **2011**, *477*, 304−307.
(29) Ren, Z.; Taskin, A. A.; Sasaki, S.; Segawa, K.; Ando, Y. *Phys. Rev. B* **2012**, *85*, 155301.
(30) Cha, J. J.; Kong, D.; Hong, S.-S.; Analytis, J. G.; Lai, K.; Cui, Y. *Nano Lett.* **2012**, *12*, 1107−1111.
(31) Garate, I.; Glazman, L. *Phys. Rev. B* **2012**, *86*, 035422.
(32) Steinberg, H.; Lalo, J.-B.; Fatemi, V.; Moodera, J. S.; Jarillo-Herrero, P. *Phys. Rev. B* **2011**, *84*, 233101.
(33) Bansal, N.; Kim, Y. S.; Brahlek, M.; Edrey, E.; Oh, S. *Phys. Rev. Lett.* **2012**, *109*, 116804.
(34) Kim, Y. S.; Brahlek, M.; Bansal, N.; Edrey, E.; Kapilevich, G. A.; Iida, K.; Tanimura, M.; Horibe, Y.; Cheong, S.-W.; Oh, S. *Phys. Rev. B* **2011**, *84*, 073109.
(35) Lu, H.-Z.; Shen, S.-Q. *Phys. Rev. B* **2011**, *84*, 125138.
(36) Xiong, J.; Luo, Y.; Khoo, Y.; Jia, S.; Cava, R. J.; Ong, N. P. *Phys. Rev. B* **2012**, *86*, 045314.
(37) Taskin, A. A.; Sasaki, S.; Segawa, K.; Ando, Y. *Phys. Rev. Lett.* **2012**, *109*, 066803.
(38) Zyuzin, A. A.; Hook, M. D.; Burkov, A. A. *Phys. Rev. B* **2011**, *83*, 245428.
(39) Pershoguba, S. S.; Yakovenko, V. M. *Phys. Rev. B* **2012**, *86*, 165404.
(40) Chen, J.; He, X. Y.; Wu, K. H.; Ji, Z. Q.; Lu, L.; Shi, J. R.; Smet, J. H.; Li, Y. Q. *Phys. Rev. B* **2011**, *83*, 241304(R).
(41) Liu, M.; Chang, C.-Z.; Zhang, Z.; Zhang, Y.; Ruan, W.; He, K.; Wang, L.-l.; Chen, X.; Jia, J.-F.; Zhang, S.-C.; Xue, Q.-K.; Ma, X.; Wang, Y. *Phys. Rev. B* **2011**, *83*, 165440.
(42) Takagaki, Y.; Jenichen, B.; Jahn, U.; Ramsteiner, M.; Friedland, K.-J. *Phys. Rev. B* **2012**, *85*, 115314.